

# Entanglement and Many-Body effects in Collective Neutrino Oscillations

Alessandro Roggero<sup>1</sup>

<sup>1</sup>*InQubator for Quantum Simulation (IQuS), Department of Physics,  
University of Washington, Seattle, WA 98195, USA*

(Dated: February 23, 2021)

Collective neutrino oscillations play a crucial role in transporting lepton flavor in astrophysical settings, such as supernovae, where the neutrino density is large. In this regime, neutrino-neutrino interactions are important and simulations in mean-field approximations show evidence for collective oscillations occurring at time scales much larger than those associated with vacuum oscillations. In this work, we study the out-of-equilibrium dynamics of a corresponding spin model using Matrix Product States and show how collective bipolar oscillations can be triggered by quantum fluctuations if appropriate initial conditions are present. The origin of these flavor oscillations, absent in the mean-field, can be traced to the presence of a dynamical phase transition, which drastically modifies the real-time evolution of the entanglement entropy. We find entanglement entropies scaling at most logarithmically in the system size suggesting that classical tensor network methods could be efficient in describing collective neutrino dynamics more generally.

Neutrinos play a pivotal role in extreme astrophysical events like core-collapse supernovae and neutron star mergers, where they are responsible for both reinvigorating a stalled shock-wave and controlling the conditions for nucleosynthesis in the ejected material [1, 2]. In these environments with a large neutrino density  $\rho_\nu$ , neutrino flavor evolution is substantially modified by neutrino-neutrino scattering processes which can lead to self-sustained collective flavor oscillations [3–12]. Since neutrinos in supernovae are emitted with fluxes and spectra that are strongly flavor dependent [2], the presence of collective flavor oscillations could then lead to important effects [13–15]. For large neutrino densities near the proto-neutronstar, flavor oscillations can occur at frequencies of the order of the neutrino-neutrino interaction energy  $\mu = \sqrt{2}G_F\rho_\nu$  instead of the much smaller vacuum oscillation frequency  $\omega = \Delta m^2/(2E)$ , a phenomenon known as fast flavor conversion [16–19] (see [20, 21] for reviews). In these expressions  $G_F$  is Fermi’s constant,  $E$  the neutrino energy and  $\Delta m^2 = m_2^2 - m_1^2$  the mass gap in the two flavor approximation used in this work.

The standard approach to study these collective phenomena is to neglect incoherent scattering and only consider neutrino-neutrino interactions in the forward-scattering limit where only flavor can be exchanged among neutrinos. In this limit, a finite system with  $N$  neutrinos is represented as a collection of  $SU(2)$  flavor isospins governed by the Hamiltonian [22] [23]

$$H_{fs} = \sum_{k=1}^N \frac{\Delta m^2}{4E_k} \vec{B} \cdot \vec{\sigma}_k + \frac{\mu}{2N} \sum_{i<j}^N \mathcal{J}_{ij} \vec{\sigma}_i \cdot \vec{\sigma}_j, \quad (1)$$

with  $\vec{\sigma}_i = (\sigma_i^x, \sigma_i^y, \sigma_i^z)$  the vector of Pauli matrices acting on the  $i$ -th neutrino. In the expression above,  $E_k$  are the neutrino energies and, in the flavor basis  $\{|\uparrow\rangle, |\downarrow\rangle\} = \{|\nu_e\rangle, |\nu_x\rangle\}$ , the orientation of the (normalized) vector  $\vec{B} = (\sin(2\theta), 0, -\cos(2\theta))$  is related to the mixing angle  $\theta$ . The geometry of the problem is encoded

in the two-body coupling matrix  $\mathcal{J}_{ij} = (1 - \hat{p}_i \cdot \hat{p}_j)$  with  $\hat{p}_k = \vec{p}_k/|\vec{p}_k|$  and  $\vec{p}_k$  the momentum of the  $k$ -th neutrino.

The current understanding of fast collective oscillations is that they are caused by unstable modes in the mean field approximation of the dynamics generated by the Hamiltonian in Eq. (1) which can amplify initially small flavor perturbations exponentially fast [19, 20, 24]. The role of entanglement and quantum effects in the out-of-equilibrium dynamics of neutrinos has received renewed interest recently [25, 26] but is still not well understood, with seemingly conflicting results in the past predicting either a vanishingly small contribution in the large system size limit [27, 28] or substantial flavor evolution over time scales  $\tau_F = \mu^{-1} \log(N)$ , which can remain relevant for realistically sized systems [24, 29].

In this work, we study the model Eq. (1) for large systems in a simplifying limit and show how coherent flavor oscillations at the fast scale  $\tau_F$  can occur when the system undergoes a dynamical phase transition [30–32], even without vacuum mixing. In the next section we introduce the details of model and initial conditions and present the results of our simulations. We then conclude with a summary on the possible implications of our work.

## NEUTRINO SPIN MODEL

We consider a simple model, in the mass basis, in which the neutrinos are divided into two equally sized “beams” ( $A$  and  $B$ ) and initialized as the following product state

$$|\Psi_0\rangle = \left( \bigotimes_{n=1}^{N/2} |\downarrow\rangle \right) \otimes \left( \bigotimes_{m=1}^{N/2} |\uparrow\rangle \right). \quad (2)$$

This corresponds to choosing all the neutrinos in the  $A$  beam to be  $|\nu_2\rangle$  and all the neutrinos in the  $B$  beam to be  $|\nu_1\rangle$ . We will consider the simple case where the energies of the neutrinos in beam  $A$  are all equal to  $E_A$  and

similarly for the neutrinos in beam  $B$ . Finally, we will neglect the geometric information encoded in the coupling matrix  $\mathcal{J}_{ij}$  and take the single angle approximation by setting  $\mathcal{J}_{ij} = 1$  for all neutrinos [20, 22] (see also [33]).

The resulting neutrino Hamiltonian, similar to the one considered in Ref. [25], can be written as follows

$$H = -\frac{\omega_A}{2} \sum_{i \in A} \sigma_i^z - \frac{\omega_B}{2} \sum_{i \in B} \sigma_i^z + \frac{\mu}{2N} \sum_{i < j} \vec{\sigma}_i \cdot \vec{\sigma}_j, \quad (3)$$

where  $\mathcal{A}$  and  $\mathcal{B}$  are sets of indices for the neutrinos in the  $A$  and  $B$  beam respectively while we set the one body energies as  $\omega_k = \Delta m^2 / (2E_k)$ . Since our initial state is completely polarized along the  $z$ -axis, the mean field approximation for the dynamics generated by  $H$  predicts no flavor evolution at all: any time evolution of the flavor polarization is completely driven by quantum fluctuations. The Hamiltonian in Eq. (3) is integrable and a complete solution could be obtained using the Bethe ansatz [22]. This is used in Ref. [25] to study a time-dependent generalization of the model for small systems.

At this point it is convenient to introduce the total spin operator  $\vec{J} = \sum_i \vec{\sigma}_i / 2$  and correspondingly  $\vec{J}^A$  and  $\vec{J}^B$  for the neutrinos in the two beams. The full Hamiltonian in Eq. (3) commutes with both the  $z$  component of the total spin,  $J_z$ , and its magnitude,  $J^2$ . As the initial state  $|\Psi_0\rangle$  is an eigenstate of  $J_z$ , we can rewrite the relevant Hamiltonian for our setup as follows

$$H = -\delta_\omega (J_z^A - J_z^B) + \frac{\mu}{N} J^2, \quad (4)$$

where we dropped irrelevant constant factors and introduced a single parameter  $\delta_\omega = (\omega_A - \omega_B)/2$  for the energy difference between the two beams. This model is a variant of the Lipkin-Meshov-Glick (LMG) model [34] explored extensively in the past [35–39]. The model with no vacuum term merits special attention: when  $\delta_\omega = 0$  the Hamiltonian clearly conserves the total spin  $J^2$  and it's diagonal in the  $|J, M\rangle$  angular momentum basis. In this limit, exact results for the flavor dynamics can be obtained as shown in Ref. [27] (see also [28]). In this model, fast flavor oscillation are shown to occur at time scales much longer than  $\tau_F$  with the scaling  $\tau_L = \mu^{-1} \sqrt{N}$  expected from incoherent scattering from the background neutrinos [27, 40]. Due to this strong scaling with system size, for large systems with  $N \gg 1$  the flavor dynamics is essentially frozen and the mean field prediction of no evolution eventually becomes exact. This has been taken as an indication that the mean field description is appropriate for large systems and that entanglement does not play any major role [27, 40].

As a way to track flavor oscillations, we compute the probability  $p(t) = (1 - \langle \sigma_1^z(t) \rangle) / 2$  that a neutrino (we take the first) is found in the same flavor state it had in the initial state (in this case  $|\downarrow\rangle$ ), the so-called flavor persistence [27, 29]. By using the exchange symmetry for neutrinos within each beam of both the Hamiltonian and

the initial state  $|\Psi_0\rangle$ , together with energy conservation under time evolution, we can write the instantaneous expectation value of the total spin as

$$\langle J^2(t) \rangle = \frac{N}{2} \left( 1 + 2 \frac{\delta_\omega}{\mu} N (1 - p(t)) \right). \quad (5)$$

When  $\delta_\omega / \mu < 0$  the total spin, starting already at a relatively small value, can only decrease further during time evolution. Since  $J^2$  is positive semi-definite, this introduces a lower bound  $p(t) \geq 1 - \mu / (2N\delta_\omega)$  and the neutrinos remain thus frozen in the initial state in the thermodynamic limit. In the opposite limit, for  $\delta_\omega / \mu \geq 1/4$  flavor fluctuations start to become parametrically small as  $p(t) \geq 1 - \mu / (4\delta_\omega)$  but remain finite in the  $N \gg 1$  limit. In the intermediate regime  $0 < \delta_\omega / \mu \lesssim 1/4$  we instead expect to find strong flavor fluctuations.

We solve for the real-time evolution of the system using a Matrix Product State (MPS) ansatz for the many-body wave function [41–43] (see Supplemental Material for more details). The approach has a controllable error and it's computationally efficient for systems with low levels of bipartite entanglement [41, 44].

## RESULTS

The qualitative difference on the collective flavor oscillations in the different dynamical phases can be observed directly from the time evolution of the flavor polarization. In Fig. 1 we show the average flavor polarization of the neutrinos in the  $A$  beam  $\langle J_z^A(t) \rangle / (N/4) = 1 - 2p(t)$ , for a system of  $N = 96$  neutrinos and different values for the asymmetry energy  $\delta_\omega$ . Due to the conservation of  $J_z$ ,

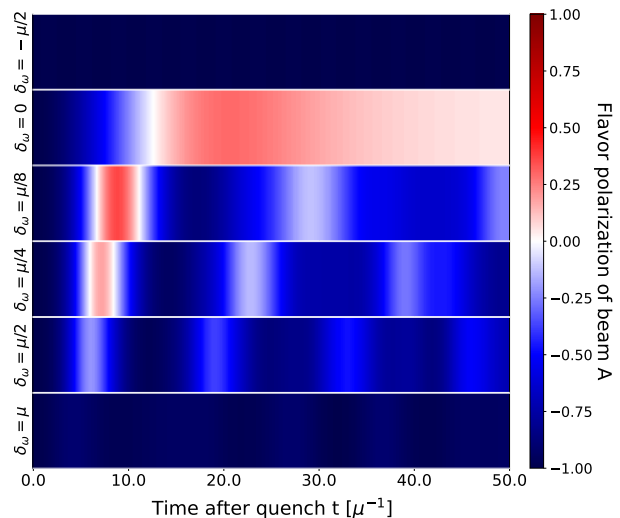


FIG. 1. (Color online) Flavor polarization per particle  $\langle J_z^A(t) \rangle / (N/4)$  of neutrinos in the  $A$  beam as a function of time for six values of the energy asymmetry parameter  $\delta_\omega / \mu$  (from top to bottom):  $-0.5, 0.0, 0.125, 0.25, 0.5, 1.0$ .

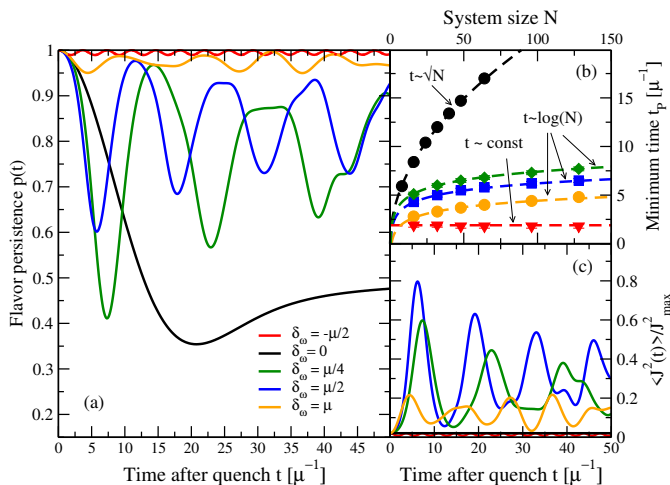


FIG. 2. (Color online) Panel (a) shows the flavor persistence  $p(t)$  in a system of  $N = 96$  neutrinos initialized in  $|\Psi_0\rangle$  and quenched at different values of the one body asymmetry parameter: the red line at the top is for a negative value  $\delta_\omega = -\mu/2$ , the black line contains only the two body potential and the green, blue and orange lines correspond to positive asymmetries  $\delta_\omega = (0.25, 0.5, 1.0)\mu$  respectively. Panel (b) shows the evolution of the minimum time  $t_P$  as a function of system size and panel (c) shows the (normalized) time dependent expectation value of the total angular momentum for different values of  $\delta_\omega$  in a system of  $N = 96$  neutrinos.

the polarization of beam B is simply the inverse. We can see strong flavor oscillations for  $0 < \delta_\omega \lesssim \mu$  which for  $\delta_\omega < \mu/2$  can even lead to a net flavor inversion in the beam (red areas in Fig. 1). In the frozen phases for large values of  $\delta_\omega/\mu$  (bottom panel) or negative asymmetries (top panel), the amplitude of these flavor fluctuations is greatly reduced. More detail on these flavor fluctuations is given in panel (a) of Fig. 2 where we show the results for the persistence  $p(t)$  and the same system of  $N = 96$  neutrinos. We see that for negative values of  $\delta_\omega$  the polarization experiences small oscillations around the initial state, as expected from our the discussion on the evolution of the total angular momentum based on Eq. (5).

In the broken phase for  $0 < \delta_\omega \lesssim \mu$  the flavor persistence experiences instead fast oscillations on time scales much shorter than in the high density limit  $\delta_\omega = 0$ . If, in the latter case, the minimum of the persistence is reached for time scales proportional to  $\tau_L \propto \sqrt{N}$ , in the former case we have instead evolution at the fast scale  $\tau_F \propto \log(N)$  found in Refs. [24, 29], but now for a physical model with  $SU(2)$  invariance (see also [45]). The logarithmic dependence on system size of the time to reach the minimum  $t_P$  is evident from the results presented in panel (b) of Fig. 2. For all values of  $\delta_\omega \neq 0$  a good fit to data is obtained with the ansatz  $\mu t_P(N) = a_t \log(N) + c_t$ . The best fit values for the parameters extracted from our simulations are reported in Tab. I, together with the extrapolated value of the minimum of the persistence  $p_{min}$

$\delta_\omega/\mu$	$a_t$	$b_t$	$c_t$	$p_{min}$
-0.5	0	0	1.8(2)	1.00(1)
0.0	0	2.10(5)	0	0.36(1)
0.01	5.4(2)	0	-8(1)	0.35(2)
0.05	2.58(6)	0	0	0.31(4)
0.125	1.65(6)	0	1.4(2)	0.32(3)
0.25	1.22(4)	0	1.6(2)	0.41(3)
0.5	1.06(4)	0	1.4(2)	0.61(4)
1.0	0.96(5)	0	0	0.99(2)

TABLE I. Optimal parameters of the model discussed in the main text  $\mu t_P(N) = a_t \log(N) + b_t \sqrt{N} + c_t$  for time to reach the minimum of the persistence  $t_P$ . The minimum of the persistence in the thermodynamic limit is extracted using the ansatz  $p_{min}(N) = p_{min} + p_c/N^\gamma$  with exponents  $\gamma = 1$  for  $\delta_\omega = 0$  and  $\gamma = 0.5$  otherwise.

in the  $N \gg 1$  limit. In particular we see that, for  $\delta_\omega$  outside the critical region  $(0.0, 1.0)$ , the latter converges to  $p_{min} \approx 1$  in the thermodynamic limit and no flavor evolution is present. Interestingly, the fluctuation timescales in the unstable region seem to scale approximately as  $a_t \propto \sqrt{\mu/\delta_\omega}$  similarly to the more familiar bipolar oscillations [46–48]. The instability observed in our simulations is also similar to bipolar oscillations in that, if we take the beam  $B$  to be composed of anti-neutrinos (with negative  $\omega_B$  [20] in normal hierarchy) and beam  $A$  of neutrinos, the appearance of the dynamical phase transition leading to oscillations in our setting depends on the neutrino hierarchy: for inverted hierarchy, the single particle energies change sign (accounting for  $\Delta m^2 < 0$ ) and the dynamical phase transition cannot occur because  $\delta_\omega < 0$  irrespective of the energies, for normal hierarchy we have always positive energy differences and fast oscillations can occur when  $\omega_A + |\omega_B| \lesssim \mu$ . The situation is reversed exchanging neutrinos with anti-neutrinos. Finally, fast oscillations can also occur if both beams are composed by neutrinos (or anti-neutrinos) provided that

$$0 \leq \pm \frac{E_B - E_A}{E_A E_B} \lesssim \frac{4\sqrt{2}G_F \rho_\nu}{\Delta m^2}, \quad (6)$$

with  $+$  for  $\nu$  and  $-$  for  $\bar{\nu}$  in the normal hierarchy [49].

In panel (c) of Fig. 2 we show the, normalized, expectation value of the total angular momentum measured using the relation in Eq. (5) derived above. We use  $J_{max}^2 = N(N+2)/4$  as normalization constant. As we can see in Fig. 2, in the unstable region the system can acquire a considerable fraction of the maximum possible total angular momentum, especially for  $\delta_\omega = \mu/2$  (blue line) where it reaches a maximum of  $\approx 80\%$ . The time evolution of the different components of the total angular momentum can be related directly to the evolution of entanglement in the many body state generated by the dynamics using spin squeezing inequalities [50–52]. In particular, using the generalized inequalities of Ref. [51], together with the conditions  $\langle \vec{J}(t) \rangle = \langle J_z^2(t) \rangle = 0$  valid at any point in the time evolution, we see that any value

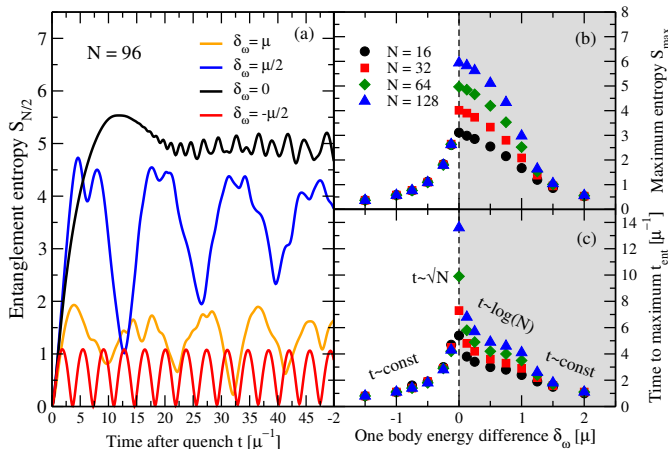


FIG. 3. (Color online) Half chain entanglement entropy  $S_{N/2}$  for  $N = 96$  neutrinos and different values of the one-body energy difference: the orange line is  $\delta_\omega = \mu$ , the blue line is for  $\delta_\omega = \mu/2$ , the red line for  $\delta_\omega = -\mu/2$  and the black line has  $\delta_\omega = 0$ . Panel (b) shows the maximum entropy  $S_{max}$  for three system sizes  $N = 16, 32, 64, 128$  and different values of  $\delta_\omega$ . Panel (c) shows the time  $t_{ent}$  to reach the maximum.

of  $\langle J^2 \rangle$  that deviates from the initial value of  $N/2$  implies entanglement. The maximum violation for smaller values of  $J^2$ , explored in the dynamics with  $\delta_\omega/\mu < 0$ , is obtained for singlet states with zero total spin and variance [52, 53]. Higher values of total angular momentum, as obtained in the unstable region, are related instead to symmetric Dicke states with  $m$  excitations [52, 54].

As an alternative way to quantify quantum correlations in the evolved state, we compute the half-chain entanglement entropy (see eg. [55]) defined explicitly as

$$S_{N/2}(t) = -Tr [\rho_B(t) \log_2(\rho_B(t))] . \quad (7)$$

Here the density matrix  $\rho_B = Tr_A [\rho(t)]$  is obtained by tracing the full density matrix  $\rho(t) = |\Psi(t)\rangle\langle\Psi(t)|$  of the system at time  $t$  over the first  $N/2$  neutrinos.

The presence of different dynamical phases can be seen directly from the results on the half-chain entanglement entropy  $S_{N/2}(t)$  presented in Fig. 3. Panel (b) shows the maximum value  $S_{max}$  that is reached by the entanglement entropy for different values of  $\delta_\omega$  and system sizes while in panel (a) we show examples of the time evolution of  $S_{N/2}(t)$  for a system of  $N = 96$  neutrinos. In the frozen phase, for  $\delta_\omega < 0$ , the behavior is similar to a gapped system with  $S_{max}$  independent of system size while we find  $S_{N/2}(t)$  to oscillate in time (red curve) with an approximately constant frequency. We recover a similar result for  $\delta_\omega \gtrsim \mu$  when, as expected from the discussion above, the system becomes again approximately frozen in the initial configuration. As shown in panel (a) for the case  $\delta_\omega = \mu$  (orange line), the oscillations in the entanglement entropy are much less regular than in the frozen phase and do not return close to zero. At the transition point  $\delta_\omega = 0$  we find that, after an initial rapid

growth phase, the entropy  $S_{N/2}(t)$  reaches a peak at  $S_{max} \approx \log_2(N/2)$  and then plateaus at a slightly smaller value with oscillations around the average. This maximum value for the entanglement entropy is reminiscent to the one in ground states of spin systems at a quantum critical point [56, 57] and reflects the absence of a gap in the Hamiltonian. We find a similar behavior for the maximum entropy reached in the dynamics for the intermediate regime  $0 < \delta_\omega/\mu \lesssim 1$  as shown in panel (b). For non-zero values of the energy asymmetry however, the half-chain entanglement entropy  $S_{N/2}(t)$  shows strong oscillations analogous to those found in similar spin models undergoing a dynamical phase transition [45]. We note that an increased dynamics of the entanglement entropy has been already associated in the past to the presence of a dynamical phase transition, but was usually associated with a increase of the time-derivative of  $S_{N/2}$  at the critical times [58, 59].

The time  $t_{ent}$  needed to reach the first maximum in the entanglement entropy is shown in panel (c) of Fig. 3 and has three distinct scaling regimes: for  $\delta_\omega < 0$  is approximately independent from system size, at the critical point we recover the familiar  $t_P \approx \sqrt{N}$  and for positive  $\delta_\omega > 0$  we find a logarithmic evolution  $t_P \approx \log(N)$  which seems to approach a constant again for large value of  $\delta_\omega$ . The system seems to enter a second gapped phase in this regime but simulations with larger systems might be required to confirm this.

We note at this point that the slow increase of entanglement entropy with system size (and with time) is precisely what allows us to perform a computationally tractable approximation to the time evolution using Matrix Product States [41, 44].

## SUMMARY AND PERSPECTIVE

Entanglement is a fundamental feature of interacting quantum many body systems [55, 56] which, somewhat surprisingly, can be shown to play no important role in determining ground-state properties of systems with all-to-all interactions like for the neutrino forward-scattering Hamiltonian of Eq. (1) (see eg. [60]). This is at the heart of the expectation that a mean-field treatment of the dynamics would also be appropriate. However, the role played by entanglement in out-of-equilibrium settings, like those relevant for flavor evolution in a supernova environment, is not as well understood [25, 26].

In this work we have solved for the real time dynamics of a simpler system described by the Hamiltonian in Eq. (3) sharing many similarities to the model used to describe bipolar oscillations [20, 47]. In order to overcome the exponential complexity of a direct solution of the problem we use a simple technique, based on a MPS representation [41], whose computational complexity scales with the amount of entanglement generated by the dy-

namics. The results for the simple model described by the integrable Hamiltonian in Eq. (3) suggest that the maximum bipartite entropy reached in fast neutrino oscillations scales only as  $\log(N)$  with the logarithm of the system size. This favorable scaling allows for the efficient calculation of the dynamics for relatively long times and systems exceeding 100 neutrinos. The computational efficiency could also be improved by using more complex tensor network states like MERA [61] which naturally describe states with logarithmically increasing entropy.

As shown in the accompanying paper [45], the behavior observed here is also found in similar (non-integrable) spin systems whose out-of-equilibrium dynamics crosses a quantum critical point, suggesting a strong link between dynamical phase transitions and fast collective oscillations. This link provides us directly with conditions, like Eq. (6), to determine when instabilities can occur. These conditions provide a generalization of those commonly obtained with linear stability analysis to the long time, non-linear, regime.

The artificial setting considered here, with a strongly asymmetric initial state and no vacuum mixing effect, was chosen to highlight differences with a typical mean-field treatment of the problem where the dynamics is simply absent. We expect however the qualitative conclusions reached here, fast oscillations caused by a dynamical phase transition and a general slow growth of the entanglement entropy with system size, to be valid also in more general situations where both multi-angle effects and more complicated energy distributions are considered [45]. In this regime, MPS simulations could be used reliably to track flavor dynamics up to relatively large, and more realistic, neutrino systems.

Based on the results presented here, we still cannot completely exclude the existence of neutrino configurations able to generate substantially more entanglement during the dynamics. Interestingly, the presence of these classically-hard configurations would be signalled clearly by the failure of the MPS method to scale efficiently to large system sizes. If found, these would be ideal models to explore using near-term quantum simulators like trapped-ion systems [62] or future circuit based quantum computers [63], which do not necessarily suffer from an exponentially increasing computational cost when large entanglement is present. In future studies, the effects discussed here will be integrated into more realistic simulations to better ascertain the role of entanglement in the dynamical evolution of dense neutrino environments of astrophysical importance.

I want to thank Joseph Carlson, Vincenzo Cirigliano, Huaiyu Duan, Joshua Martin, Amol Patwardhan, Ermal Rrapaj and Martin Savage for the many useful discussions about the subject of this work. This work was supported by the InQubator for Quantum Simulation under U.S. DOE grant No. DE-SC0020970 and by the Quantum Science Center (QSC), a National Quantum Infor-

mation Science Research Center of the U.S. Department of Energy (DOE).

- 
- [1] R. D. Hoffman, S. E. Woosley, and Y.-Z. Qian, “Nucleosynthesis in neutrino-driven winds. II. implications for heavy element synthesis,” *The Astrophysical Journal* **482**, 951–962 (1997).
  - [2] Hans-Thomas Janka, “Explosion mechanisms of core-collapse supernovae,” *Annual Review of Nuclear and Particle Science* **62**, 407–451 (2012).
  - [3] Martin J. Savage, Robert A. Malaney, and George M. Fuller, “Neutrino Oscillations and the Leptonic Charge of the Universe,” *Astrophys. J.* **368**, 1 (1991).
  - [4] James Pantaleone, “Dirac neutrinos in dense matter,” *Phys. Rev. D* **46**, 510–523 (1992).
  - [5] James Pantaleone, “Neutrino oscillations at high densities,” *Physics Letters B* **287**, 128 – 132 (1992).
  - [6] Sergio Pastor and Georg Raffelt, “Flavor oscillations in the supernova hot bubble region: Nonlinear effects of neutrino background,” *Phys. Rev. Lett.* **89**, 191101 (2002).
  - [7] A B Balantekin and H Yüksel, “Neutrino mixing and nucleosynthesis in core-collapse supernovae,” *New Journal of Physics* **7**, 51–51 (2005).
  - [8] George M. Fuller and Yong-Zhong Qian, “Simultaneous flavor transformation of neutrinos and antineutrinos with dominant potentials from neutrino-neutrino forward scattering,” *Phys. Rev. D* **73**, 023004 (2006).
  - [9] Huaiyu Duan, George M. Fuller, J. Carlson, and Yong-Zhong Qian, “Coherent development of neutrino flavor in the supernova environment,” *Phys. Rev. Lett.* **97**, 241101 (2006).
  - [10] Alexander Friedland, “Self-refraction of supernova neutrinos: Mixed spectra and three-flavor instabilities,” *Phys. Rev. Lett.* **104**, 191102 (2010).
  - [11] Joshua D. Martin, Changhao Yi, and Huaiyu Duan, “Dynamic fast flavor oscillation waves in dense neutrino gases,” *Physics Letters B* **800**, 135088 (2020).
  - [12] Meng-Ru Wu and Irene Tamborra, “Fast neutrino conversions: Ubiquitous in compact binary merger remnants,” *Phys. Rev. D* **95**, 103007 (2017).
  - [13] Gianluigi Fogli, Eligio Lisi, Antonio Marrone, and Alessandro Mirizzi, “Collective neutrino flavor transitions in supernovae and the role of trajectory averaging,” *Journal of Cosmology and Astroparticle Physics* **2007**, 010–010 (2007).
  - [14] Yong-Zhong Qian, George M. Fuller, Grant J. Mathews, Ron W. Mayle, James R. Wilson, and S. E. Woosley, “Connection between flavor-mixing of cosmologically significant neutrinos and heavy element nucleosynthesis in supernovae,” *Phys. Rev. Lett.* **71**, 1965–1968 (1993).
  - [15] Yong-Zhong Qian and George M. Fuller, “Neutrino-neutrino scattering and matter-enhanced neutrino flavor transformation in supernovae,” *Phys. Rev. D* **51**, 1479–1494 (1995).
  - [16] R. F. Sawyer, “Speed-up of neutrino transformations in a supernova environment,” *Phys. Rev. D* **72**, 045003 (2005).
  - [17] R. F. Sawyer, “Neutrino cloud instabilities just above the neutrino sphere of a supernova,” *Phys. Rev. Lett.* **116**,

- 081101 (2016).
- [18] S. Chakraborty, R. S. Hansen, I. Izaguirre, and G.G. Raffelt, “Self-induced neutrino flavor conversion without flavor mixing,” *Journal of Cosmology and Astroparticle Physics* **2016**, 042–042 (2016).
- [19] Ignacio Izaguirre, Georg Raffelt, and Irene Tamborra, “Fast pairwise conversion of supernova neutrinos: A dispersion relation approach,” *Phys. Rev. Lett.* **118**, 021101 (2017).
- [20] Huaiyu Duan, George M. Fuller, and Yong-Zhong Qian, “Collective neutrino oscillations,” *Annual Review of Nuclear and Particle Science* **60**, 569–594 (2010), <https://doi.org/10.1146/annurev.nucl.012809.104524>.
- [21] Sovan Chakraborty, Rasmus Hansen, Ignacio Izaguirre, and Georg Raffelt, “Collective neutrino flavor conversion: Recent developments,” *Nuclear Physics B* **908**, 366 – 381 (2016), neutrino Oscillations: Celebrating the Nobel Prize in Physics 2015.
- [22] Y. Pehlivan, A. B. Balantekin, Toshitaka Kajino, and Takashi Yoshida, “Invariants of collective neutrino oscillations,” *Phys. Rev. D* **84**, 065008 (2011).
- [23] Note the difference in the definition of  $\mu$  there.
- [24] R.F. Sawyer, “‘Classical’ instabilities and ‘quantum’ speed-up in the evolution of neutrino clouds,” (2004), [arXiv:hep-ph/0408265](https://arxiv.org/abs/hep-ph/0408265).
- [25] Michael J. Cervia, Amol V. Patwardhan, A. B. Balantekin, S. N. Coppersmith, and Calvin W. Johnson, “Entanglement and collective flavor oscillations in a dense neutrino gas,” *Phys. Rev. D* **100**, 083001 (2019).
- [26] Ermal Rrapaj, “Exact solution of multiangle quantum many-body collective neutrino-flavor oscillations,” *Phys. Rev. C* **101**, 065805 (2020).
- [27] Alexander Friedland and Cecilia Lunardini, “Do many-particle neutrino interactions cause a novel coherent effect?” *Journal of High Energy Physics* **2003**, 043–043 (2003).
- [28] Alexander Friedland, Bruce H. J. McKellar, and Ivona Okuniewicz, “Construction and analysis of a simplified many-body neutrino model,” *Phys. Rev. D* **73**, 093002 (2006).
- [29] Nicole F. Bell, Andrew A. Rawlinson, and R.F. Sawyer, “Speed-up through entanglement—many-body effects in neutrino processes,” *Physics Letters B* **573**, 86 – 93 (2003).
- [30] Martin Eckstein, Marcus Kollar, and Philipp Werner, “Thermalization after an interaction quench in the hubbard model,” *Phys. Rev. Lett.* **103**, 056403 (2009).
- [31] Bruno Sciolla and Giulio Biroli, “Dynamical transitions and quantum quenches in mean-field models,” *Journal of Statistical Mechanics: Theory and Experiment* **2011**, P11003 (2011).
- [32] Bruno Sciolla and Giulio Biroli, “Quantum quenches, dynamical transitions, and off-equilibrium quantum criticality,” *Phys. Rev. B* **88**, 201110 (2013).
- [33] Since  $[H, J_A^2] = [H, J_B^2] = 0$  we are free to change the intra-beam couplings at will thus changing the geometry. In the general case we can substitute  $\mu \rightarrow \mu(1 - \cos(\theta_{AB}))$ , with  $\theta_{AB}$  the angle between the momenta in the  $A$  and  $B$  beams, for all the results in this work.
- [34] H.J. Lipkin, N. Meshkov, and A.J. Glick, “Validity of many-body approximation methods for a solvable model: (i). exact solutions and perturbation theory,” *Nuclear Physics* **62**, 188 – 198 (1965).
- [35] Julien Vidal, Rémy Mosseri, and Jorge Dukelsky, “Entanglement in a first-order quantum phase transition,” *Phys. Rev. A* **69**, 054101 (2004).
- [36] Julien Vidal, Guillaume Palacios, and Claude Aslangul, “Entanglement dynamics in the lipkin-meshkov-glick model,” *Phys. Rev. A* **70**, 062304 (2004).
- [37] Julien Vidal, Guillaume Palacios, and Rémy Mosseri, “Entanglement in a second-order quantum phase transition,” *Phys. Rev. A* **69**, 022107 (2004).
- [38] José I. Latorre, Román Orús, Enrique Rico, and Julien Vidal, “Entanglement entropy in the lipkin-meshkov-glick model,” *Phys. Rev. A* **71**, 064101 (2005).
- [39] Pedro Ribeiro, Julien Vidal, and Rémy Mosseri, “Exact spectrum of the lipkin-meshkov-glick model in the thermodynamic limit and finite-size corrections,” *Phys. Rev. E* **78**, 021106 (2008).
- [40] Alexander Friedland and Cecilia Lunardini, “Neutrino flavor conversion in a neutrino background: Single- versus multi-particle description,” *Phys. Rev. D* **68**, 013007 (2003).
- [41] Guifré Vidal, “Efficient classical simulation of slightly entangled quantum computations,” *Phys. Rev. Lett.* **91**, 147902 (2003).
- [42] Guifré Vidal, “Efficient simulation of one-dimensional quantum many-body systems,” *Phys. Rev. Lett.* **93**, 040502 (2004).
- [43] Sebastian Paegel, Thomas Köhler, Andreas Swoboda, Salvatore R. Manmana, Ulrich Schollwöck, and Claudius Hubig, “Time-evolution methods for matrix-product states,” *Annals of Physics* **411**, 167998 (2019).
- [44] Norbert Schuch, Michael M. Wolf, Frank Verstraete, and J. Ignacio Cirac, “Entropy scaling and simulability by matrix product states,” *Phys. Rev. Lett.* **100**, 030504 (2008).
- [45] A. Roggero, “Dynamical phase transitions in models of collective neutrino oscillations,” (in preparation (2021)).
- [46] V. Alan Kostelecký and Stuart Samuel, “Self-maintained coherent oscillations in dense neutrino gases,” *Phys. Rev. D* **52**, 621–627 (1995).
- [47] Steen Hannestad, Georg G. Raffelt, Günter Sigl, and Yvonne Y. Y. Wong, “Self-induced conversion in dense neutrino gases: Pendulum in flavor space,” *Phys. Rev. D* **74**, 105010 (2006).
- [48] Huaiyu Duan, George M. Fuller, J. Carlson, and Yong-Zhong Qian, “Analysis of collective neutrino flavor transformation in supernovae,” *Phys. Rev. D* **75**, 125005 (2007).
- [49] Note that this condition can be modified by the presence of an MSW-like matter term which couple differently to the two flavors.
- [50] A. Sørensen, L.-M. Duan, J. I. Cirac, and P. Zoller, “Entanglement in a second-order quantum phase transition,” *Nature* **409**, 63–66 (2001).
- [51] Géza Tóth, Christian Knapp, Otfried Gühne, and Hans J. Briegel, “Optimal spin squeezing inequalities detect bound entanglement in spin models,” *Phys. Rev. Lett.* **99**, 250405 (2007).
- [52] Géza Tóth, Christian Knapp, Otfried Gühne, and Hans J. Briegel, “Spin squeezing and entanglement,” *Phys. Rev. A* **79**, 042334 (2009).
- [53] Géza Tóth, “Entanglement detection in optical lattices of bosonic atoms with collective measurements,” *Phys. Rev. A* **69**, 052327 (2004).
- [54] John K. Stockton, J. M. Geremia, Andrew C. Doherty, and Hideo Mabuchi, “Characterizing the entanglement

- of symmetric many-particle spin- $\frac{1}{2}$  systems,” Phys. Rev. A **67**, 022112 (2003).
- [55] J. Eisert, M. Cramer, and M. B. Plenio, “Colloquium: Area laws for the entanglement entropy,” Rev. Mod. Phys. **82**, 277–306 (2010).
- [56] G. Vidal, J. I. Latorre, E. Rico, and A. Kitaev, “Entanglement in quantum critical phenomena,” Phys. Rev. Lett. **90**, 227902 (2003).
- [57] G. Refael and J. E. Moore, “Entanglement entropy of random quantum critical points in one dimension,” Phys. Rev. Lett. **93**, 260602 (2004).
- [58] Markus Heyl, “Dynamical quantum phase transitions: a review,” Reports on Progress in Physics **81**, 054001 (2018).
- [59] Asmi Haldar, Krishnanand Mallayya, Markus Heyl, Frank Pollmann, Marcos Rigol, and Arnab Das, “Signatures of quantum phase transitions after quenches in quantum chaotic one-dimensional systems,” arXiv e-prints, arXiv:2004.02905 (2020), arXiv:2004.02905 [cond-mat.stat-mech].
- [60] Fernando G. S. L. Brandão and Aram W. Harrow, “Product-state approximations to quantum states,” Communications in Mathematical Physics **342**, 47–80 (2016).
- [61] G. Vidal, “Class of quantum many-body states that can be efficiently simulated,” Phys. Rev. Lett. **101**, 110501 (2008).
- [62] J. Zhang, G. Pagano, P. W. Hess, A. Kyprianidis, P. Becker, H. Kaplan, A. V. Gorshkov, Z.-X. Gong, and C. Monroe, “Observation of a many-body dynamical phase transition with a 53-qubit quantum simulator,” Nature **551**, 601–604 (2017).
- [63] B. Hall, A. Roggero, A. Baroni, and J. Carlson, “Quantum simulation of collective neutrino oscillations,” (in preparation (2021)).
- [64] Ulrich Schollwöck, “The density-matrix renormalization group in the age of matrix product states,” Annals of Physics **326**, 96 – 192 (2011), January 2011 Special Issue.
- [65] F. Verstraete and J. I. Cirac, “Matrix product states represent ground states faithfully,” Phys. Rev. B **73**, 094423 (2006).
- [66] Masuo Suzuki, “General theory of fractal path integrals with applications to many-body theories and statistical physics,” Journal of Mathematical Physics **32**, 400–407 (1991).
- [67] E M Stoudenmire and Steven R White, “Minimally entangled typical thermal state algorithms,” New Journal of Physics **12**, 055026 (2010).
- [68] Ian D. Kivlichan, Jarrod McClean, Nathan Wiebe, Craig Gidney, Alán Aspuru-Guzik, Garnet Kin-Lic Chan, and Ryan Babbush, “Quantum simulation of electronic structure with linear depth and connectivity,” Phys. Rev. Lett. **120**, 110501 (2018).
- [69] Matthew Fishman, Steven R. White, and E. Miles Stoudenmire, “The ITensor software library for tensor network calculations,” (2020), arXiv:2007.14822.

### Matrix Product State Simulation

In this supplemental material we provide a self-contained explanation of the Matrix Product State (MPS) technique used to generate the results in this

work. Additional information can be found in the original paper [41] and in more recent reviews [43, 64]. In order to implement long-range interactions efficiently with a MPS, we use the same strategy introduced recently for circuit based simulations in [63], a brief explanation of the construction is presented in the last subsection.

### MPS Representation

Consider a general quantum state  $|\Psi\rangle$  of a system with  $N$  spin-1/2 particle, it’s wavefunction can be expressed as a rank- $N$  tensor as

$$|\Psi\rangle = \sum_{\sigma_1, \dots, \sigma_N} \Psi^{\sigma_1 \dots \sigma_N} |\sigma_1 \dots \sigma_N\rangle, \quad (8)$$

with  $|\sigma_1 \dots \sigma_N\rangle$  one of the  $2^N$  basis states spanning the total Hilbert space of the system. A Matrix Product State is an exact representation of the rank- $N$  tensor  $\Psi^{\sigma_1 \dots \sigma_N}$  as a product of  $N$ , smaller, rank-3 tensors  $M_{\alpha, \beta}^{\sigma_k}$ . A constructive procedure to find this representation, starting from the original tensor  $\Psi^{\sigma_1 \dots \sigma_N}$ , can be obtained by applying  $N$  times a Singular Value Decomposition (SVD) of appropriately reshaped tensors. This decomposition allows to represent an arbitrary rectangular matrix  $M$  of dimension  $D_A \times D_B$  as the following product of three matrices

$$M_{ij} = \sum_k U_{ik} \Sigma_{kk} V_{kj}^\dagger, \quad (9)$$

where  $U$  is a  $D_A \times \min(D_A, D_B)$  matrix with orthonormal columns,  $\Sigma$  is a diagonal matrix of dimension  $\min(D_A, D_B) \times \min(D_A, D_B)$  with either zero or positive entries and  $V^\dagger$  is a  $\min(D_A, D_B) \times D_B$  matrix with orthonormal rows. An important property of the SVD, which we will use repeatedly in the derivation below, is that the approximation of the original matrix  $M$ , with rank  $r \leq \min(D_A, D_B)$ , using a second matrix  $M'$  with rank  $r' < r$  can be done optimally, in the Frobenius norm, by truncating the sum in Eq. (9) so that we keep only the  $r'$  largest singular values  $\Sigma_{kk}$ . We will assume that the SVD is performed with the convention that singular values in  $\Sigma$  are ordered as  $\Sigma_{11} \geq \dots \geq \Sigma_{NN}$ . With this convention, the optimal approximation corresponds to truncating the sum as

$$M'_{ij} = \sum_k^{r'} U_{ik} \Sigma_{kk} V_{kj}^\dagger. \quad (10)$$

Starting from the first spin on the left, we first reshape  $\Psi^{\sigma_1 \dots \sigma_N}$  into the rectangular matrix  $\Psi_{\sigma_1(\sigma_2 \dots \sigma_N)}$  of dimension  $2 \times 2^{N-1}$ . A SVD of this matrix will then

produce the following decomposition

$$\begin{aligned}
\Psi_{\sigma_1(\sigma_2 \cdots \sigma_N)} &= \sum_{\alpha_1}^{r_1} U_{\sigma_1 \alpha_1} \Sigma_{\alpha_1 \alpha_1} V_{\alpha_1(\sigma_2 \cdots \sigma_N)}^\dagger \\
&= \sum_{\alpha_1}^{r_1} U_{\sigma_1 \alpha_1} W_{\alpha_1 \sigma_2 \cdots \sigma_N} \\
&= \sum_{\alpha_1}^{r_1} A_{\alpha_1}^{[1] \sigma_1} \Psi_{(\alpha_1 \sigma_2)(\sigma_3 \cdots \sigma_N)}^{[1]},
\end{aligned} \tag{11}$$

with  $r_1 \leq 2$  the rank of the original rectangular matrix and in the second line we have reshaped the product of  $\Sigma$  and  $V^\dagger$  to a vector  $\vec{W}$ . In the last line, we have further reshaped the matrix  $U$  into two row vectors, with components  $A_{\alpha_1}^{[1] \sigma_1} = U_{\sigma_1 \alpha_1}$ , and the vector  $\vec{W}$  to a  $2r_1 \times 2^{N-2}$  matrix  $\Psi_{(\alpha_1 \sigma_2)(\sigma_3 \cdots \sigma_N)}^{[1]}$ . At this point, we can repeat the procedure by applying a SVD to this last matrix and proceed from left to right until we have reached the last spin of the chain. The resulting decomposition becomes

$$\begin{aligned}
\Psi^{\sigma_1 \cdots \sigma_N} &= \sum_{\alpha_1, \dots, \alpha_{N-1}} A_{\alpha_1}^{[1] \sigma_1} A_{\alpha_1 \alpha_2}^{[2] \sigma_2} \dots A_{\alpha_{N-2} \alpha_{N-1}}^{[N-1] \sigma_{N-1}} A_{\alpha_{N-1}}^{[N] \sigma_N} \\
&= \mathbf{A}^{[1] \sigma_1} \mathbf{A}^{[2] \sigma_2} \dots \mathbf{A}^{[N-1] \sigma_{N-1}} \mathbf{A}^{[N] \sigma_N},
\end{aligned} \tag{12}$$

where in the last line we suppressed the lower indices and replaced them by matrix multiplications. Using this construction, a general state  $|\Psi\rangle$  can be written as a Matrix Product State. Note that the rank of the SVD in the center of the chain could be as large as  $2^{N/2-1}$  (assuming  $N$  even) and storage requirements for representing a general state will then scale exponentially with the system size.

As we will see soon, the maximum rank  $r_{max} = \max_k r_k$  needed to describe accurately a given state is related to the maximum bipartite entanglement entropy in the system. In order to see this, it is first useful to introduce a different construction for the MPS. Consider a similar iterative decomposition procedure for the tensor  $\Psi^{\sigma_1 \cdots \sigma_N}$  as the one described above, but now starting from the right-most site. The first step leads to

$$\begin{aligned}
\Psi_{(\sigma_1 \cdots \sigma_{N-1}) \sigma_N} &= \sum_{\beta_N}^{r_N} U_{(\sigma_1 \cdots \sigma_{N-1}) \beta_N} \Sigma_{\beta_N \beta_N} V_{\beta_N \sigma_N}^\dagger \\
&= \sum_{\beta_N}^{r_N} W'_{\sigma_1 \cdots \sigma_{N-1} \beta_N} V_{\beta_N \sigma_N}^\dagger \\
&= \sum_{\beta_N}^{r_N} \Psi_{(\sigma_1 \cdots \sigma_{N-2})(\sigma_{N-1} \beta_N)}^{[N]} B_{\beta_N}^{[N] \sigma_N},
\end{aligned} \tag{13}$$

where we have introduced the two column vectors  $B_{\beta_N}^{[N] \sigma_N} = V_{\beta_N \sigma_N}^\dagger$  and the residual matrix has maximum dimensions given by  $2^{N-2} \times 2r_N$ . Proceeding with the same procedure until the left edge, we find another matrix product state with amplitudes

$$\Psi^{\sigma_1 \cdots \sigma_N} = \mathbf{B}^{[1] \sigma_1} \mathbf{B}^{[2] \sigma_2} \dots \mathbf{B}^{[N-1] \sigma_{N-1}} \mathbf{B}^{[N] \sigma_N}. \tag{14}$$

The two representations are related by a gauge transformation [43, 64], and they are characterized by different normalization properties. In particular, we have

$$\sum_{\sigma_k} \mathbf{A}^{[k] \sigma_k \dagger} \mathbf{A}^{[k] \sigma_k} = \mathbb{1} \quad \sum_{\sigma_k} \mathbf{B}^{[k] \sigma_k} \mathbf{B}^{[k] \sigma_k \dagger} = \mathbb{1}. \tag{15}$$

For this reason, the state resulting from the decomposition in Eq. (12) in terms of  $\mathbf{A}$  tensors is called a *left-canonical* MPS, while the construction in terms of  $\mathbf{B}$  tensors in Eq. (14) is called *right-canonical* [43, 64].

In order to see more clearly the connection between entanglement and the maximum rank in the decomposition, also called *bond dimension*, it is useful to introduce yet another canonical form. This is obtained by starting with a decomposition from the left up to a chosen site  $k$ , at this point we start with a decomposition from the right and we stop when we reach site  $k+1$ . We can write the result of this decomposition as

$$\Psi^{\sigma_1 \cdots \sigma_N} = \mathbf{A}^{[1] \sigma_1} \dots \mathbf{A}^{[k] \sigma_k} \Sigma^{[k]} \mathbf{B}^{[k+1] \sigma_{k+1}} \dots \mathbf{B}^{[N] \sigma_N}, \tag{16}$$

with the diagonal matrix  $\Sigma^{[k]}$  containing the singular values at the bond between the  $k$  and the  $k+1$  sites. The site  $k$  is called the *orthogonality center*, since tensors to the left are left-normalized while tensors on the right are right-normalized. This property allows us to write the state in this representation as

$$|\Psi\rangle = \sum_{\alpha_k}^{r_k} \Sigma_{\alpha_k \alpha_k}^{[k]} |\Phi_{\alpha_k}^L\rangle \otimes |\Phi_{\alpha_k}^R\rangle, \tag{17}$$

where we have defined two sets of states

$$|\Phi_{\alpha_k}^L\rangle = \sum_{\sigma_1, \dots, \sigma_k} \left[ \mathbf{A}^{[1] \sigma_1} \dots \mathbf{A}^{[k] \sigma_k} \right]_{1 \alpha_k} |\sigma_1 \cdots \sigma_k\rangle, \tag{18}$$

and

$$|\Phi_{\alpha_k}^R\rangle = \sum_{\sigma_{k+1}, \dots, \sigma_N} \left[ \mathbf{B}^{[k+1] \sigma_{k+1}} \dots \mathbf{B}^{[N] \sigma_N} \right]_{\alpha_k 1} |\sigma_{k+1} \cdots \sigma_N\rangle. \tag{19}$$

Thanks to the normalization properties of the  $\mathbf{A}$  and  $\mathbf{B}$  tensors from Eq. (15), we see that these states form orthonormal sets of states for the left and right Hilbert spaces respectively. We can then interpret Eq. (17) as the Schmidt decomposition of the state  $|\Psi\rangle$  on the left-right bipartition. The number of states in the sum can then be identified with the *Schmidt rank*, which is a natural measure of entanglement between states on the left partition and states on the right one.

In particular, the Von-Neumann entanglement entropy for the left-right bipartition at site  $k$  of the state  $|\Psi\rangle$  can be expressed as a function of the singular values as

$$S_k = - \sum_{\alpha_k=1}^{r_k} \Sigma_{\alpha_k \alpha_k}^{[k]2} \log_2 \left( \Sigma_{\alpha_k \alpha_k}^{[k]2} \right). \tag{20}$$

The *Schmidt rank*  $r_k$  gives the number of non-zero singular values so that the entanglement is bounded by

$$S_k \leq \log_2(r_k). \quad (21)$$

We can now see that MPS with small bond dimensions correspond to quantum states with little entanglement [41]. Before moving on to the time-dependent simulation, it's important to mention that the *mixed-canonical* form in Eq. (16) is also particularly convenient to find more efficient approximations to an initial MPS. Given an MPS  $|\Psi\rangle$  with bond dimension  $r_k$  at the bond between site  $k$  and  $k+1$ , we can find another MPS  $|\Psi'\rangle$  with lower bond dimension  $r'_k < r_k$  so that the error in 2-norm is bounded from above by [65]

$$\| |\Psi\rangle - |\Psi'\rangle \|_2^2 \leq 2 \sum_{\alpha_k=r'_k+1}^{r_k} \Sigma_{\alpha_k}^{[k]2}. \quad (22)$$

Thanks to the bi-orthogonality of the Schmidt decomposition Eq. (17), we can obtain  $|\Psi'\rangle$  from  $|\Psi\rangle$  by keeping only the  $r'_k$  largest singular values in the sum. If the singular values decrease sufficiently fast, a good approximation to the original state could be obtained with an MPS with a much smaller bond dimension [41].

### Time evolution of a MPS

We now turn to explain how one can simulate the time-evolution for the general neutrino Hamiltonian in Eq. (1) of the main text. The basic operation we will use repeatedly in the following is the application of an  $SU(4)$  operation on a pair of nearest neighbor indices  $(k, k+1)$ . A generic  $4 \times 4$  unitary  $U$  of this type can be represented as a rank 4 tensor  $G_{\sigma'_1 \sigma'_2}^{\sigma_1 \sigma_2}$  with each index having dimension equal to 2. When we contract this tensor with the MPS, only the tensors around the bond  $(k, k+1)$  get transformed. More specifically, we have that the matrices

$$\mathbf{C}^{\sigma_k \sigma_{k+1}} = \mathbf{A}^{[k] \sigma_k} \Sigma^{[k]} \mathbf{B}^{[k+1] \sigma_{k+1}}, \quad (23)$$

get updated into

$$\tilde{\mathbf{C}}^{\sigma_k \sigma_{k+1}} = \sum_{\sigma'_k \sigma'_{k+1}} G_{\sigma'_k \sigma'_{k+1}}^{\sigma_k \sigma_{k+1}} \mathbf{A}^{[k] \sigma'_k} \Sigma^{[k]} \mathbf{B}^{[k+1] \sigma'_{k+1}}. \quad (24)$$

We can now restore the MPS form by performing one final SVD of  $\tilde{\mathbf{C}}^{\sigma_k \sigma_{k+1}}$  properly reshaped as a matrix

$$\tilde{C}_{(\alpha_{k-1} \sigma_k)(\sigma_{k+1} \beta_{k+2})} = \sum_{\alpha_k}^{\tilde{r}_k} U_{(\alpha_{k-1} \sigma_k) \alpha_k} \Sigma_{\alpha_k} \mathbf{A}^{[k] \sigma_k} V_{\alpha_k (\sigma_{k+1} \beta_{k+2})}^\dagger, \quad (25)$$

with a possibly larger bond dimension  $\tilde{r}_k$ . Now, by identifying  $\tilde{\mathbf{A}}^{[k] \sigma_k}$  with  $U$ ,  $\tilde{\mathbf{B}}^{[k+1] \sigma_{k+1}}$  with  $V^\dagger$  and the singular

vector matrices  $\tilde{\Sigma}^{[k]}$  with  $\Sigma$ , we have a new MPS with decomposition

$$\tilde{\Psi}^{\sigma_1 \dots \sigma_N} = \mathbf{A}^{[1] \sigma_1} \dots \tilde{\mathbf{A}}^{[k] \sigma_k} \tilde{\Sigma}^{[k]} \tilde{\mathbf{B}}^{[k+1] \sigma_{k+1}} \dots \mathbf{B}^{[N] \sigma_N}. \quad (26)$$

The SVD requires  $\mathcal{O}((r_{k-1} + r_{k+1})r_{k+1}^2)$  operations and is efficient only if we are able to keep a small bond dimension by truncating the MPS as shown above.

With nearest-neighbor two-site operators at our disposal, we can now present the scheme used to simulate time evolution under Hamiltonians of the form

$$H = \sum_{k=1}^N \vec{B}_k \cdot \vec{\sigma}_k + \sum_{i < j}^N \mathcal{V}_{ij} \vec{\sigma}_i \cdot \vec{\sigma}_j, \quad (27)$$

with arbitrary long range interactions. For convenience we first rewrite the Hamiltonian as a sum of, not necessarily nearest-neighbor, pair Hamiltonians  $h_{ij}$  as

$$H = \sum_{i < j}^N \left[ \frac{\vec{B}_i \cdot \vec{\sigma}_i + \vec{B}_j \cdot \vec{\sigma}_j}{N-1} + \mathcal{V}_{ij} \vec{\sigma}_i \cdot \vec{\sigma}_j \right] = \sum_{i < j}^N h_{ij}. \quad (28)$$

The time evolution operator under this Hamiltonian can be approximated for short times using

$$e^{-i\delta H} = \prod_{i < j=1}^N e^{-i\delta h_{ij}} \prod_{i < j=N}^1 e^{-i\delta h_{ij}} + \mathcal{O}(\delta^3 \|H\|^3), \quad (29)$$

where the second sequence of products are performed in reverse order. This is the standard second-order Trotter-Suzuki approximation for the time evolution operator [66]. Each one of the operators appearing in Eq. (29) is a  $SU(4)$  unitary acting on all pairs of sites for a total of  $N(N-1)$  gates. In order to replace long range gates into nearest-neighbor ones, it is convenient to introduce the SWAP operation. This is defined as

$$\text{SWAP} = \begin{pmatrix} 1 & 0 & 0 & 0 \\ 0 & 0 & 1 & 0 \\ 0 & 1 & 0 & 0 \\ 0 & 0 & 0 & 1 \end{pmatrix}. \quad (30)$$

When applied to a pair of sites, it exchanges the state as

$$\text{SWAP} |\phi\rangle \otimes |\psi\rangle = |\psi\rangle \otimes |\phi\rangle. \quad (31)$$

Using this operation we can transport two sites next to each other, apply the unitary  $T_{ij} = \exp(-i\delta h_{ij})$  as a nearest-neighbor operation and finally swap the two sites back to their original position [67]. Given the all-to-all nature of the pair interaction in Eq. (28), a naive application of this strategy will result in  $\mathcal{O}(N^3)$  nearest-neighbor operations to implement one step of time evolution using the approximation in Eq. (29) for the propagator.

In this work we employ instead the swap-network scheme introduced in Ref. [63] for studying neutrino dynamics on a digital quantum computer with linear connectivity. The construction is inspired by earlier work

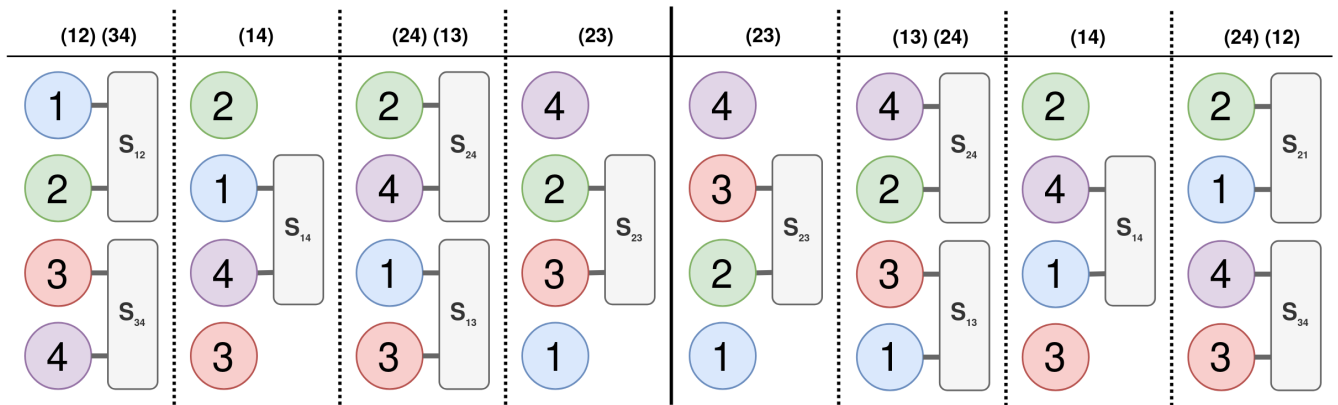


FIG. 4. (Color online) Schematic representation of one step of time evolution for a system with  $N = 4$  neutrinos. The label on the top indicate the Hamiltonian terms  $h_{ij}$  considered at each one of the  $2N = 8$  sub-steps.

on fermionic swap-networks [68] and relies on the observation that, if we perform  $N$  layers of nearest-neighbor swap operations by alternating the even bonds with the odd bonds, we can bring every site next to every other site at least once using a total of  $N(N-1)/2$  operations. At the end of these  $N$  steps, the sites will be left in reverse order. It is now clear that, if we define a modified propagator  $S_{ij}$  as follows

$$S_{ij} = \text{SWAP} \times \exp(-i\delta h_{ij}), \quad (32)$$

and apply nearest-neighbor  $S_{ij}$  operations instead of swaps as before, at the end of the sequence we will have implemented the first product of pair operators in the approximation Eq. (29) for the propagator. If we now apply the sequence in reverse order we can complete a full time step and obtain a state where sites have the original order. A schematic depiction of a complete step for a system with  $N = 4$  neutrinos is displayed in Fig. 4. In this work we perform a SVD truncation to MPS form after each application of the nearest neighbor operation using a threshold of  $10^{10}$  for the discarded eigenvalues. Better truncation schemes are possible (see eg. [43]) and their

potential advantages will be explored in future work.

Finally, we decompose the full time evolution for a total time  $t$  into steps of size  $\delta \ll t$  as

$$\exp(-itH) = [\exp(-i\delta H)]^{t/\delta}. \quad (33)$$

We then approximate each short-time propagator for time  $\delta$  using the swap-network scheme described above.

For all the results presented in the main text, we used a fixed time-step  $\delta = 0.05\mu^{-1}$  which we found provided a good compromise between precision and efficiency for the systems studied here. As already mentioned above, the overall scheme remains efficient provided the singular values on each bond decay sufficiently fast to zero that a good approximation to the MPS can be obtained using a low bond dimension. Thanks to the (at most) logarithmic scaling of the entanglement entropy observed in the systems studied in main text, the maximum bond dimension required to keep the truncation error below  $10^{-10}$  was  $\approx N/2$  allowing us to easily explore systems with  $N \gtrsim 100$ . The software developed to carry out the simulations reported in this work used the C++ version of the ITensor library which provides efficient representations for MPS and more general tensors [69].